



ZnO–PVA Polymer Matrix with Transition Metals Oxide Nano-fillers for High Dielectric Mediums

Tahir Iqbal¹ · M. Irfan¹ · Shahid M. Ramay² · Asif Mahmood³ · Murtaza Saleem⁴ · Saadat A. Siddiqi⁵

Published online: 9 June 2020

© Springer Science+Business Media, LLC, part of Springer Nature 2020

Abstract

Polymer-based nanocomposites are considered promising candidates for flexible modern electronic devices. ZnO–PVA polymer nanocomposites have gained recent research interest due to excellent optical and dielectric properties. Transition metals (Cr, Mn, Fe, Ni, Cu) oxide nanoparticles incorporated ZnO–PVA composite matrix are investigated in this work for a comprehensive study of its structure, morphology, optical and dielectric parameters. Crystallographic information revealed the presence of crystalline zinc oxide and transition metals oxides reflections in specific orientations in the PVA matrix. The inter-particle distance and interfacial interaction of transition metal oxide nanoparticles in host polymer are observed as important factors for improved dipole polarization. The nanoparticles of metal oxides in matrix induce the enhanced negative charge carriers and exhibit robust interactions with positive carriers of the polymer surface. A sharp and substantial increment in real dielectric permittivity from 74 for ZnO–PVA to maximum 350 for ZnO–PVA–Fe₂O₃ composition was observed by the addition of transition metal oxides in the PVA matrix with same loss factor value of 0.1.

Keywords Polymer nanocomposite · Optical · Dielectrics

Introduction

Polymeric matrix based on composite materials with nanoparticle fillers possesses excellent optical, mechanical, and electrical properties for advance applications like solar cells, biomedical sensors, and capacitors [1, 2]. Polymer composites with high dielectric constant are desirable mediums for noble power conversion efficiency with high charge recombination and exciton binding energy [3]. High dielectric and

robustness of polyvinyl alcohol (PVA) and zinc oxide (ZnO) composites make these excellent candidates for high performance light emitting devices [4]. ZnO nano-fillers in the PVA matrix incorporated advanced optical and electrical properties [5]. A considerable change in the band gap of PVA was experienced with the addition of ZnO nanoparticles in its matrix [6]. Optical studies of CuO substituted polymer/ZnO nanocomposites were carried out for a clear demonstration of the change in transmittance and absorption coefficient [7]. Dielectric studies of ZnO–PVA polymer nanocomposites synthesized through various emerging chemical techniques reported the maximum dielectric permittivity value approximately 104 at low-frequency regimes and retain the stability at some controlled higher temperatures which makes these suitable candidates for flexible electronic devices [8, 9]. The inter-particle distance of metal oxide nano-filler in a polymer matrix is another important factor for the improvement of dipole polarization. The nanoparticles of metal oxides in matrix induce enhanced negative charge carriers and exhibit robust interactions with positive charge carriers of the polymer surface. Meanwhile, transition metal oxides are considered excellent candidates for energy storage capacity due to having good dispensability in the polymer matrix [10–12]. ZnO is a well known

✉ Shahid M. Ramay
schaudhry@ksu.edu.sa

✉ Murtaza Saleem
murtaza.saleem@lums.edu.pk

¹ Department of Physics, Mirpur University of Science and Technology (MUST), Mirpur 10250 AJK, Pakistan

² Physics and Astronomy Department, College of Science, King Saud University, Riyadh 11451, Saudi Arabia

³ Chemical Engineering Department, College of Engineering, King Saud University, Riyadh 11451, Saudi Arabia

⁴ Department of Physics, SBASSE, Lahore University of Management Sciences, Lahore 54792, Pakistan

⁵ IRCBM, COMSATS University Islamabad, Lahore Campus, Defence Road, Off Raiwind Road, Lahore 54600, Pakistan

semiconducting material with direct energy band gap of 3.37 eV having excellent optical and electronic properties [13]. It is recently observed that only 1 wt% dispersion of ZnO nanoparticles in polymer matrix significantly stimulates the physical properties of polymer nanocomposites [14]. The dielectric permittivity in another investigation found to increase with the addition of ZnO nanoparticles in PVA [15]. On the other hand, transition metals (Cr, Mn, Fe, Ni, and Cu) oxide have incredible dielectric parameters with low energy loss values. The enhanced values of dielectric constant were reported in some transition metal oxides (Cr₂O₃, NiO, and CuO) incorporated PVA matrix [16–18]. Hence, a combination of ZnO and (Cr, Mn, Fe, Ni, and Cu) oxide in flexible composites of PVA will introduce the new optical and dielectric materials with enhanced capacitive parameters. A brief study of ZnO–PVA matrix containing transition metals (Cr, Mn, Fe, Ni, and Cu) oxide nano-fillers is carried out in this work for exploring its, structural, optical and dielectric properties. These novel polymer nanocomposites are considered excellent candidates for flexible dielectric mediums due to having excellent dielectric permittivity with comparatively low loss factors.

Experimental Method

Chemicals

Polyvinyl alcohol (PVA) beads, zinc nitrate hexahydrate [Zn(NO₃)₂·6H₂O], chromium nitrate nonahydrate [Cr(NO₃)₃·9H₂O], manganese nitrate tetrahydrate [Mn(NO₃)₂·4H₂O], ferrous nitrate nonahydrate [Fe(NO₃)₂·9H₂O], nickel nitrate hexahydrate [Ni(NO₃)₂·6H₂O], copper nitrate trihydrate [Cu(NO₃)₂·3H₂O], zinc nitrate hexahydrate [Zn(NO₃)₂·6H₂O], and citric acid were supplied by Sigma-Aldrich, USA. All the precursors were of analytical grade and used without further purification.

Synthesis of ZnO and Transition Metals (Cr, Mn, Fe, Ni, and Cu) Oxide Nanoparticles

ZnO and transition metals (Cr, Mn, Fe, Ni, and Cu) oxide nanoparticles with an average diameter around 50 nm to 100 nm were prepared through a temperature-controlled citrate pyrolysis technique. The calculated molar ratios of citric acid and required metal nitrates were taken each time in a 100 ml transparent beaker. These solutions were mixed and heated constantly using a magnetic stirrer hot plate at 100 °C until obtained thick gel and afterward dry powder of solution. These dry powder samples were then placed in a furnace for 24 h at 400 °C to get the fine phase pure powders of metal oxides.

Synthesis of Transition Metal Oxides Incorporated ZnO/PVA Matrix

The required amount of beads of PVA was dissolved in distilled water under constant stirring at 40 °C until it obtained the thick gel. The amount of ZnO nanoparticles was taken as 0.5 wt% in all compositions. The synthesized transition metal oxides (Cr₂O₃, Mn₂O₃, Fe₂O₃, NiO, and CuO) with 0.5 wt% for each were homogeneously mixed in equal amounts with ultrasonic agitation to get the same approximate thickness of 0.3 ± 0.01 mm. These gels were spread in flat crucibles and placed in a furnace at 40 °C for 6 h. The final products of ZnO–PVA and transition metals oxides containing ZnO–PVA nanocomposites were obtained in the form of dry plain sheets. These sheets were cut into dimensions of 1 cm in both length and width.

Characterizations

ZnO/PVA and transition metals oxides containing ZnO–PVA nanocomposites were investigated for structural studies using the Panalytical X'Pert Multipurpose diffractometer (MPD) by employing Cu K_α X-rays using a wavelength of 0.154 nm. Morphology of samples was examined through FEI Nano-SEM 450 field emission scanning electron microscopy (FESEM) using built-in high resolution through lens detector (TLD) and scanning transmission electron microscope (STEM) detector. The elemental composition of synthesized nanoparticles and dispersive nanocomposite polymer matrices were performed using the Oxford X'Act energy dispersive X-ray spectrometer (EDS) instrument. The optical absorbance spectra were acquired using a UV–Vis spectrophotometer and corresponding band gap values extracted employing Tauc plot curves. Quadtech Precision 1910 LCR meter was used for dielectric measurements with high accuracy. The samples were placed between the Teflon cell containing polished copper electrodes. Each electrode was connected with the low and high current and potential connections of LCR meter. The capacitance C_p and loss factor (tanδ) were recorded as a function of frequency in the range of 100 to 1 MHz with a sweep step size of 50 Hz.

Results and Discussions

Crystallographic Studies

Figure 1 presents the XRD patterns of ZnO–PVA and transition metals (Cr, Mn, Fe, Ni, and Cu) oxide containing ZnO/PVA polymer nanocomposites. XRD analysis was carried out in detail using X'Pert High Score software and standard JCPD

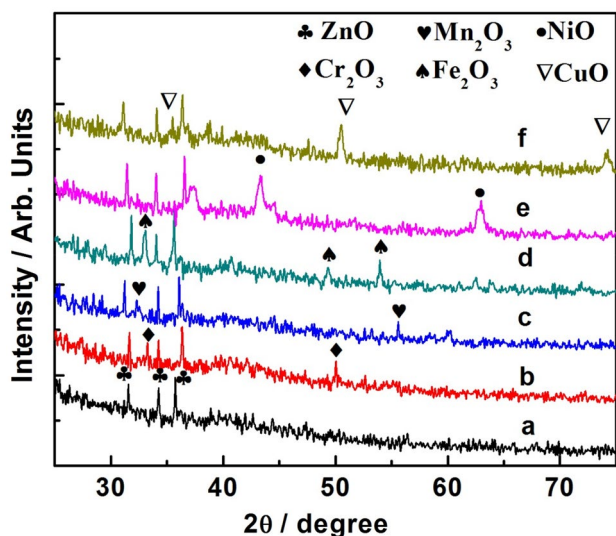


Fig. 1 XRD patterns of transition metals oxide nanoparticles incorporated PVA–ZnO polymer nanocomposites

data set for corresponding compositions. XRD spectra were also acquired of synthesized nanoparticles of ZnO and transition metals oxides before the dispersion in the ZnO–PVA matrix for checking out the phase purity and crystal structure. Rietveld refinement was performed using X’Pert High Score Plus software for each XRD spectra and results are configured in Fig. 2. The crystallographic information about cell parameters, atomic positions, Wyckoff positions, and profile R-factors were acquired and mention in Table 1. The least-square approach was used for the minimization of differences

in structural parameters of observed and simulation diffraction patterns. The difference was optimized through profile R-factors like R_{exp} , weighted R -profile (R_{wp}), R -profile (R_p), and R -Bragg (R_B) [19]. These parameters can be defined as:

$$R_{exp} = \left[\frac{N - P}{\sum_i w_i (I_o)^2} \right]^{1/2}, \quad (1)$$

$$R_{wp} = \left[\frac{\sum_i w_i (I_c - I_o)^2}{\sum_i w_i (I_o)^2} \right]^{1/2}, \quad (2)$$

$$R_p = \frac{\sum |I(O_i) - I(C_i)|}{\sum |I(O_i)|}, \quad (3)$$

$$R_B = \frac{\sum |I(O) - I(C)|}{\sum |I(O)|}, \quad (4)$$

where I_c and I_o are the calculated and observed integrated intensities, while N and P denote for the number of observed profile points and the number of refined parameters, respectively. Further, the goodness of fit GOF (χ^2) can be calculated using the following relation;

$$GOF = \frac{R_{wp}}{R_{exp}}. \quad (5)$$

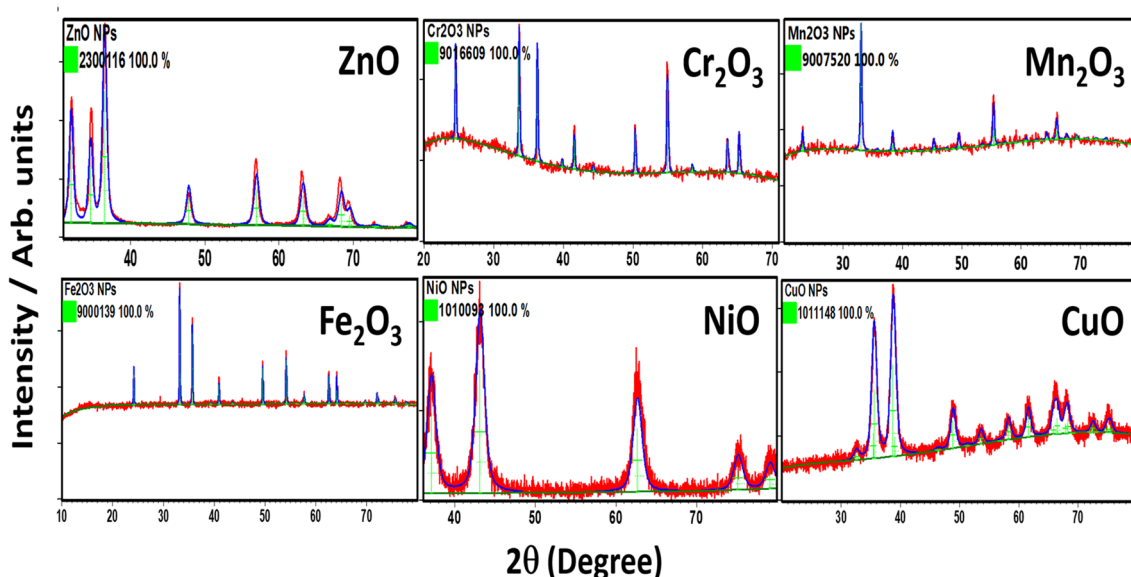


Fig. 2 Rietveld refined XRD spectra of synthesized nanoparticles present the accurate matching of points of plane reflections with standard crystallographic data

Table 1 Cell parameters, atomic positions, Wyckoff positions and Profile R-factors of synthesized nanoparticles crystal structures after Rietveld refinement

Samples	Cell parameters	Atoms	Atomic positions			Wyckoff positions	Profile R-Factor
			x	y	z		
ZnO	$a = 3.231 \text{ \AA}$	Zn	0.333	0.667	0	2b	$R_{exp} = 5.203, R_p = 12.974$
	$c = 5.181 \text{ \AA}$	O	0.333	0.667	0.381	2b	$R_{wp} = 16.237, R_B = 7.360$ $\chi^2 = 3.121, D_{stats} = 0.110$
Cr ₂ O ₃	$a = 4.952 \text{ \AA}$	Cr	0	0	0.152	12c	$R_{exp} = 4.402, R_p = 3.453$
	$b = 4.952 \text{ \AA}$	O	0.305	0	0.250	18e	$R_{wp} = 4.569, R_B = 4.627$
	$c = 13.581 \text{ \AA}$						$\chi^2 = 1.038, D_{stats} = 1.403$
Mn ₂ O ₃	$a = 9.400 \text{ \AA}$	Mn ₁	0	0	0.500	4b	$R_{exp} = 3.329, R_p = 2.469$
	$b = 9.396 \text{ \AA}$	Mn ₂	0	0	0	4a	$R_{wp} = 3.164, R_B = 2.073$
	$c = 9.400 \text{ \AA}$	Mn ₃	0.006	0.253	0.215	8c	$\chi^2 = 0.950, D_{stats} = 1.962$
		Mn ₄	0.254	0.285	0.005	8c	
		Mn ₅	0.214	0.001	0.253	8c	
		O ₆	0.150	0.415	0.132	8c	
		O ₇	0.085	0.129	0.356	8c	
		O ₈	0.375	0.353	0.419	8c	
		O ₉	0.355	0.082	0.374	8c	
		O ₁₀	0.419	0.372	0.149	8c	
		O ₁₁	0.134	0.147	0.086	8c	
Fe ₂ O ₃	$a = 5.013 \text{ \AA}$	Fe	0	0	0.145	12c	$R_{exp} = 1.694, R_p = 1.335$
	$b = 5.013 \text{ \AA}$	O	0.305	0	0.250	18e	$R_{wp} = 1.737, R_B = 1.045$
	$c = 13.736 \text{ \AA}$						$\chi^2 = 1.025, D_{stats} = 1.661$
NiO	$a = 4.192 \text{ \AA}$	Ni ₁	0.500	0.500	0.500	4b	$R_{exp} = 27.79, R_p = 23.083$
	$b = 4.192 \text{ \AA}$	O1	0	0	0	4a	$R_{wp} = 31.370, R_B = 7.487$
	$c = 4.192 \text{ \AA}$						$\chi^2 = 1.128, D_{stats} = 1.305$
CuO	$a = 4.677 \text{ \AA}$	Cu1	0.250	0.250	0	4c	$R_{exp} = 6.978, R_p = 6.094$
	$b = 3.419 \text{ \AA}$	O ₁	0	0.084	0.250	4e	$R_{wp} = 7.634, R_B = 2.854$
	$c = 5.137 \text{ \AA}$						$\chi^2 = 1.094, D_{stats} = 1.480$

XRD spectra of ZnO–PVA polymer nanocomposite compositions were indexed using the JCPD card number 00-001-1136 of the wurtzite ZnO standard pattern for observation of detected plane reflections. XRD pattern of PVA/ZnO contains three prominent peaks at 2θ values of 31.51, 34.26 and 35.71 associated with the most intense 110, 002, and 101 plane reflections of ZnO, respectively. These peaks have low intensities due to the amorphous host PVA matrix. Transition metal oxides containing ZnO/PVA compositions comprise some additional peaks along various specific orientations with ZnO reflections attributed to the presence of other crystalline nanoparticles in the matrix. These XRD peaks appeared at 2θ values of 33.51 and 50.08 (indexed with 104 and 024) of rhombohedral Cr₂O₃, 32.28 and 55.61 (indexed with 222 and 440) of cubic Mn₂O₃, 33.11, 35.71, 49.35 and 54.04 (indexed with 104, 110, 024 and 116) of rhombohedral Fe₂O₃, 43.42 and 63.10 (indexed with 200 and 220) of cubic NiO, 35.50 and 75.12 (indexed with 111 and 004) of monoclinic CuO phases matched with standard XRD spectra of corresponding compositions. This crystallographic information along with standard JCPD data set numbers are given in Table 2. A significant change in peak shift,

d-spacing, and full width at half maximum (FWHM) were observed in the most intense diffraction peak with the incorporation of transition metal oxide nanoparticles in structure. Crystallite size for each composition was measured using well known Scherrer's formula [20], by considering these parameters and calculated values along with cell volume, and atomic packing fraction (APF) mentioned in Table 3.

Morphological Analysis

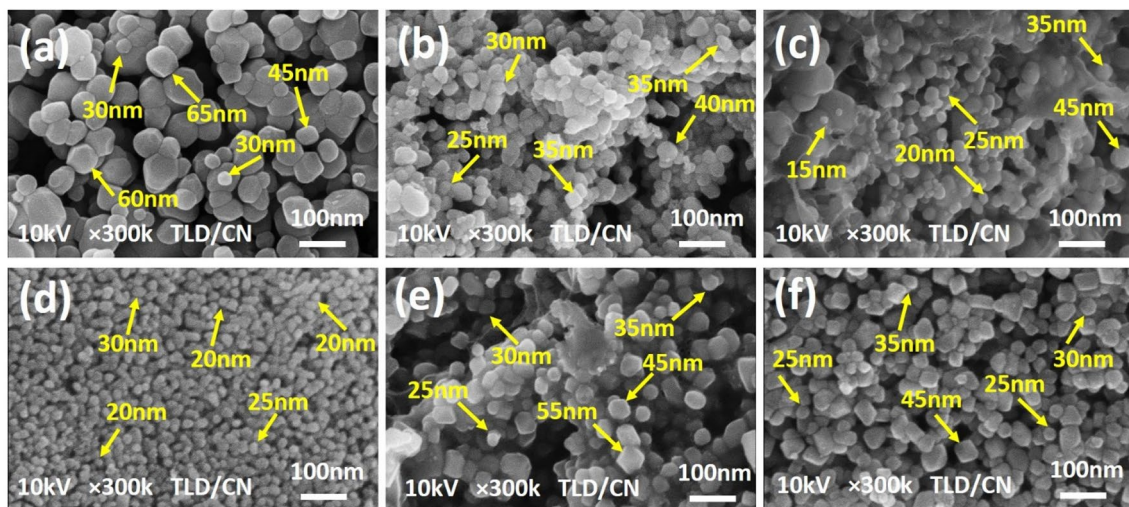
The morphology of synthesized nanoparticles and polymer nanocomposites was studied with field emission scanning electron microscopy using a TLD and STEM detector. FESEM and STEM micrographs were obtained with 10 kV beam energy at a working distance of approximately 5 mm. Figure 3 presents the micrographs of synthesized ZnO and transition metals oxide nanoparticles. The size of ZnO nanoparticles was observed in the range of 25–100 nm while the size of transition metals oxide nanoparticles found slightly smaller in the range of 15–60 nm. Average particle sizes for ZnO, Cr₂O₃, Mn₂O₃, Fe₂O₃, NiO, and CuO nanoparticles are estimated approximately as 45 nm, 35 nm, 25 nm, 35

Table 2 Crystallographic parameters of polymer nanocomposites with standard JCPD data set

Sample	Structure type	2θ	Miller indices	$d_{spacing}$ (Å)	JCPD Ref. #
ZnO–PVA	Wurtzite hexagonal	31.51	100	2.81	00-001-1136
		34.26	002	2.61	
		35.71	101	2.46	
ZnO–PVA–Cr ₂ O ₃	Rhombohedral	33.51	104	2.61	00-001-1294
		36.33	110	2.47	
		50.08	024	1.81	
ZnO–PVA–Mn ₂ O ₃	Cubic	32.28	222	2.68	00-001-1061
		55.6	440	1.66	
ZnO–PVA–Fe ₂ O ₃	Rhombohedral	33.11	104	2.69	00-001-1053
		35.71	110	2.51	
		49.35	024	1.84	
ZnO–PVA–NiO	Cubic	54.04	116	1.69	00-001-1239
		43.42	200	2.08	
ZnO–PVA–CuO	Monoclinic	63.10	220	1.47	00-001-1117
		35.50	111	2.51	
		75.12	004	1.26	

Table 3 Different parameters of polymer nanocomposites (a) ZnO–PVA, (b) ZnO–PVA–Cr₂O₃, (c) ZnO–PVA–Mn₂O₃, (d) ZnO–PVA–Fe₂O₃, (e) ZnO–PVA–NiO, and (f) ZnO–PVA–CuO

Parameters	ZnO/PVA	ZnO/PVA/Cr ₂ O ₃	ZnO/PVA/Mn ₂ O ₃	ZnO/PVA/Fe ₂ O ₃	ZnO/PVA/NiO	ZnO/PVA/CuO
Crystallite size (nm)	7.20	5.69	11.44	5.83	7.54	7.88
Lattice strain (%)	0.170	0.209	0.111	0.211	0.159	0.154
APF (g/cm ³)	0.753	0.440	1.208	0.440	1.208	1.100
Cell volume (Å) ³	46.80	288.15	719.28	299.45	63.80	96.00
Band gap (eV)	5.34	4.89	5.02	4.68	4.81	5.16
AC-conductivity (S/cm × 10 ⁻⁴)	1.1	1.8	4.1	4.6	1.7	5.15
Real part (E')	74	85	275	350	80	275
Imaginary part (E'')	0.1	0.24	250	375	225	250
Loss factor (tanδ)	0.10	0.25	0.90	0.10	2.90	0.90

**Fig. 3** FESEM micrographs of synthesized transition metals oxide nanoparticles **a** ZnO, **b** Cr₂O₃, **c** Mn₂O₃, **d** Fe₂O₃, **e** NiO, and **f** CuO

nm, and 30 nm, respectively. Most of the nanoparticles contain spherical or distorted spherical uniform distributions. Iron oxide nanoparticles are observed comparatively smaller and more uniform concerning shape, size, and distribution.

FESEM and STEM micrographs of transition metals oxide nanoparticles incorporated ZnO–PVA matrices are presented in Figs. 4 and 5, respectively. It can be observed from all micrographs that ZnO and transition metal oxide

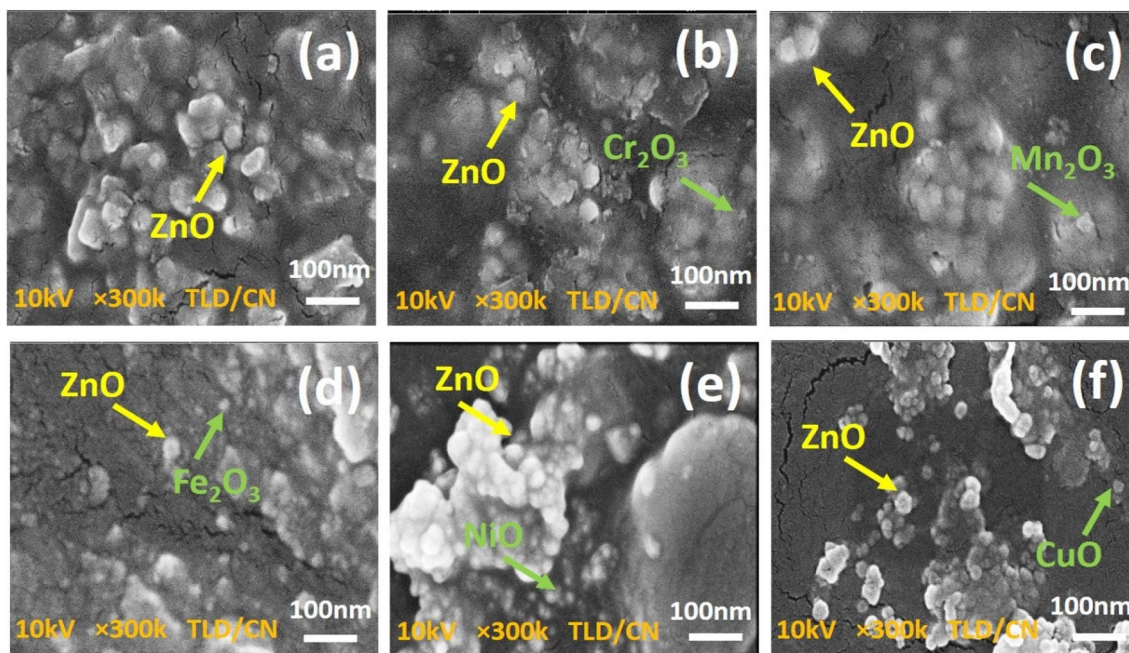


Fig. 4 FESEM micrographs of synthesized transition metals oxide nanoparticles incorporated ZnO–PVA polymer nanocomposite **a** ZnO–PVA, **b** ZnO–PVA–Cr₂O₃, **c** ZnO–PVA–Mn₂O₃, **d** ZnO–PVA–Fe₂O₃, **e** ZnO–PVA–NiO, and **f** ZnO–PVA–CuO

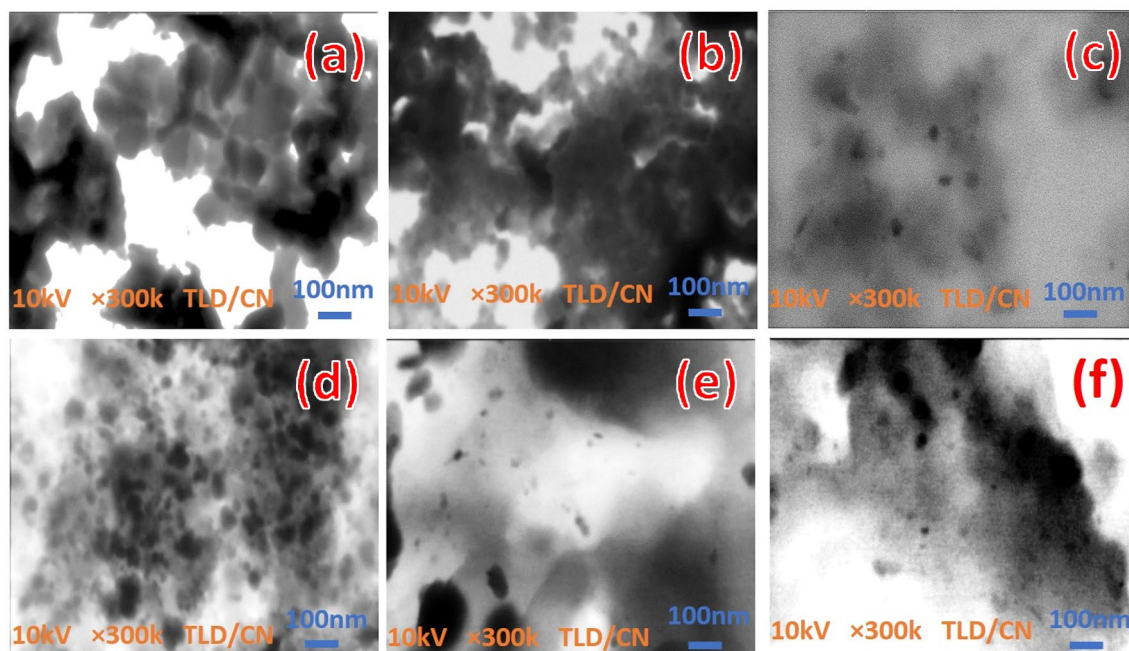


Fig. 5 FESEM micrographs of synthesized transition metals oxide nanoparticles incorporated ZnO–PVA polymer nanocomposite **a** ZnO–PVA, **b** ZnO–PVA–Cr₂O₃, **c** ZnO–PVA–Mn₂O₃, **d** ZnO–PVA–Fe₂O₃, **e** ZnO–PVA–NiO, and **f** ZnO–PVA–CuO

nanoparticles distributed evenly in the host matrix. Most of the nanoparticles have retained the original shape after dispersion in the matrix. FESEM and STEM micrographs

of iron oxide containing composition again show a more uniform distribution.

Elemental Composition Analysis

Elemental compositions of synthesized nanoparticles and polymer nanocomposites were confirmed using EDX analysis. EDX spectra were obtained with 15 kV beam energy for obtaining maximum X-ray counts. Figure 6 presents the EDX spectra of ZnO and transition metals oxide nanoparticles revealed the presence of expected nominal elemental contents in each composition without the detection of any un-necessary impurities. Gold (Au) and palladium (Pd) traces were appeared due to the implication of Au/Pd coating on samples using sputter coater before FESEM analysis. EDX spectra of polymer nanocomposites are given in Fig. 7 with zoomed insets for smaller peaks showing the intense carbon content in all compositions associated with the carbon chain of host PVA polymeric matrix. EDS spectra of transition metal oxides containing compositions reveal the presence of Cr, Mn, Fe, Ni and Cu contents with expected approximate amounts in respective polymer nanocomposites.

Optical Properties

UV–Vis spectrophotometry was employed to evaluate the optical properties of synthesized polymer nano-composites. The absorption spectra and band gap estimation using the Tauc plot for pure and transition metal oxide nanoparticles

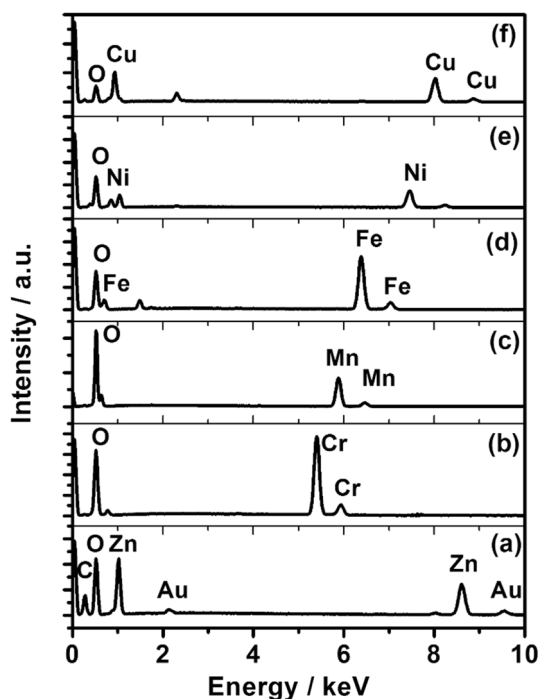


Fig. 6 EDX spectra of synthesized transition metals oxide nanoparticles (a) ZnO, (b) Cr₂O₃, (c) Mn₂O₃, (d) Fe₂O₃, (e) NiO, and (f) CuO

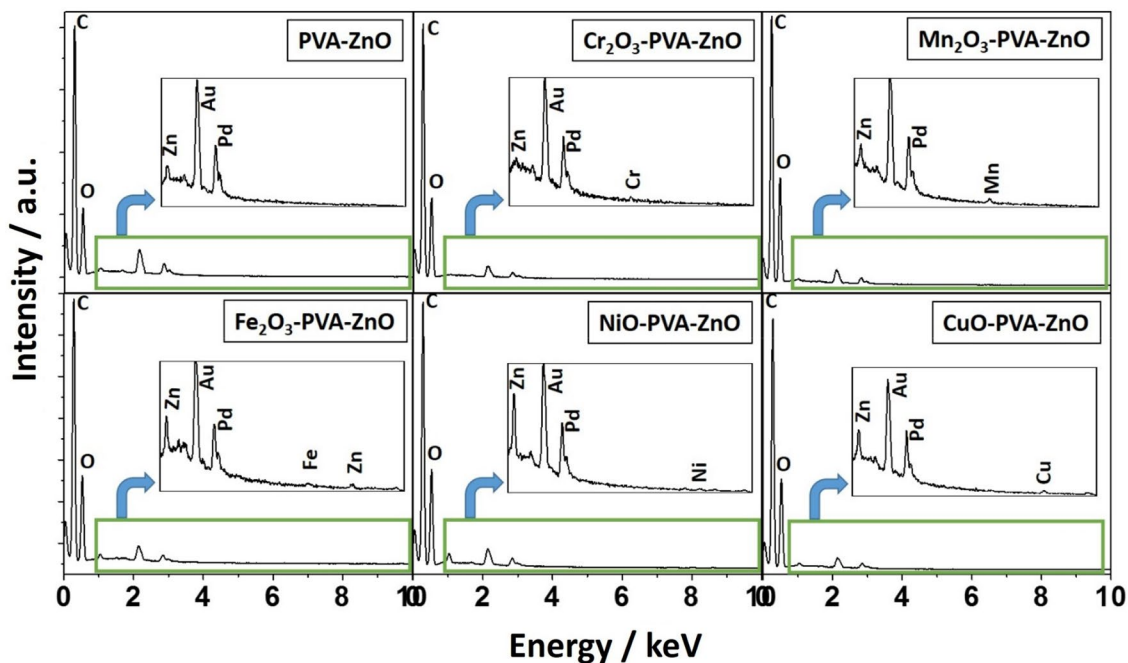


Fig. 7 EDX spectra of transition metals incorporated ZnO–PVA polymer nanocomposites

incorporated PVA–ZnO is presented in Fig. 8a, b. These composites seem active in the ultraviolet region in the wavelength range of 200–700 nm. The absorbance spectra of polymer nanocomposites were found to decrease in the energy range up to 5.5 eV and then increase exponentially in the energy range of 5.5–6.35 eV. Again a sharp decrease in absorbance was observed at higher energy ranges after 6.5 eV in all compositions. The analysis of the optical band gap is the most important parameter especially for crystalline materials to investigate the conduction mechanism in structure. The optical band gap of synthesized polymer composites were translated by Tauc's plot [21] through following equation using frequency dependent absorption spectra.

$$(\alpha h\nu)^n = B(h\nu - E_g), \quad (6)$$

where α , $h\nu$, B and E_g denote for absorption coefficient, photon energy, interband transition probability parameter,

and optical band gap, respectively. While n presents the type of electronic transition which value can take as 1/2, 3/2, 2, or 3 for direct or indirect allowed and forbidden transitions, respectively. The absorption coefficient " α ", can be acquired using the following Beer–Lambert's equation [22].

$$\alpha = \frac{2.303A}{d}, \quad (7)$$

where 'A' and 'd' presents the absorbance and thickness of the sample, respectively. The optical band gap of polymer composites were estimated using the direct electronic transition $(\alpha h\nu)^2$ due to the presence of ZnO and transition metal oxide nanoparticles in matrix. The corresponding values of optical band gap were extracted by extra plotting the tangent on x-axis as shown in Fig. 8b. The energy band gap of ZnO–PVA was observed as 5.34 eV which is in a close approximation of already reported results [23–25]. The band gap was found to decrease with the addition of transition metal oxide nanoparticles in the ZnO–PVA polymer matrix. It was reported that nanoparticles act as conductive interconnections between the polymer chains that caused an increase of the electrical conductance of the nano-composites and hence lead to a diminution in their optical band gap [26, 27]. This decrease was observed consistent with the band gap values of corresponding transition metal oxide compositions and found associated with the induction of new levels in the energy gaps that lead up the movement of electrons from the valence band to the interesting levels of the conduction band, consequently increase the conductivity. The minimum band gap value of 4.68 eV was estimated in iron oxide nanoparticles incorporated composition attributed to the availability of more carriers in the matrix for conduction mechanism.

Dielectric Measurements

Polymer nanocomposite matrix needs an excellent dielectric medium for applications in a wide range of flexible capacitive devices. Dielectric permittivity measurements were performed using a precise LCR meter with the variation of frequency. Figure 9 shows the response of dielectric permittivity and loss factor variations with the change in frequency while the overlay for each presents in Fig. 10. The capacitance of dielectric medium and loss factor ($\tan \delta$) can be easily measured by LCR meter with the variation of frequency. The values of real (ϵ') and imaginary (ϵ'') parts are considered an effective presentation for energy storage capacity in a dielectric medium. These can be calculated using the following relations [28, 29].

$$\epsilon' = \frac{Cd}{\epsilon_0 A}, \quad (8)$$

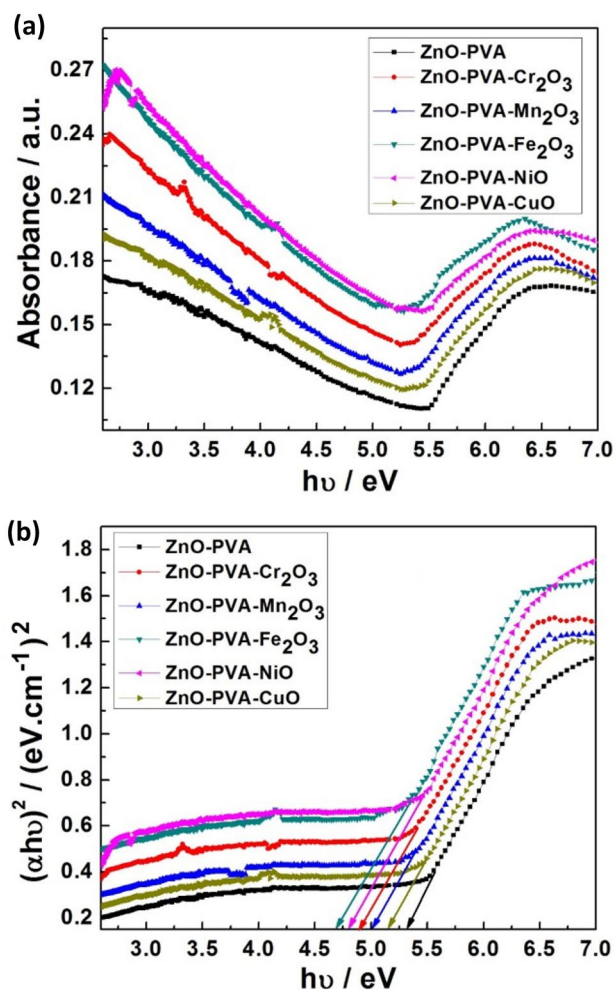


Fig. 8 Absorbance spectra and band gap estimation using Tauc plot of polymer nanocomposites

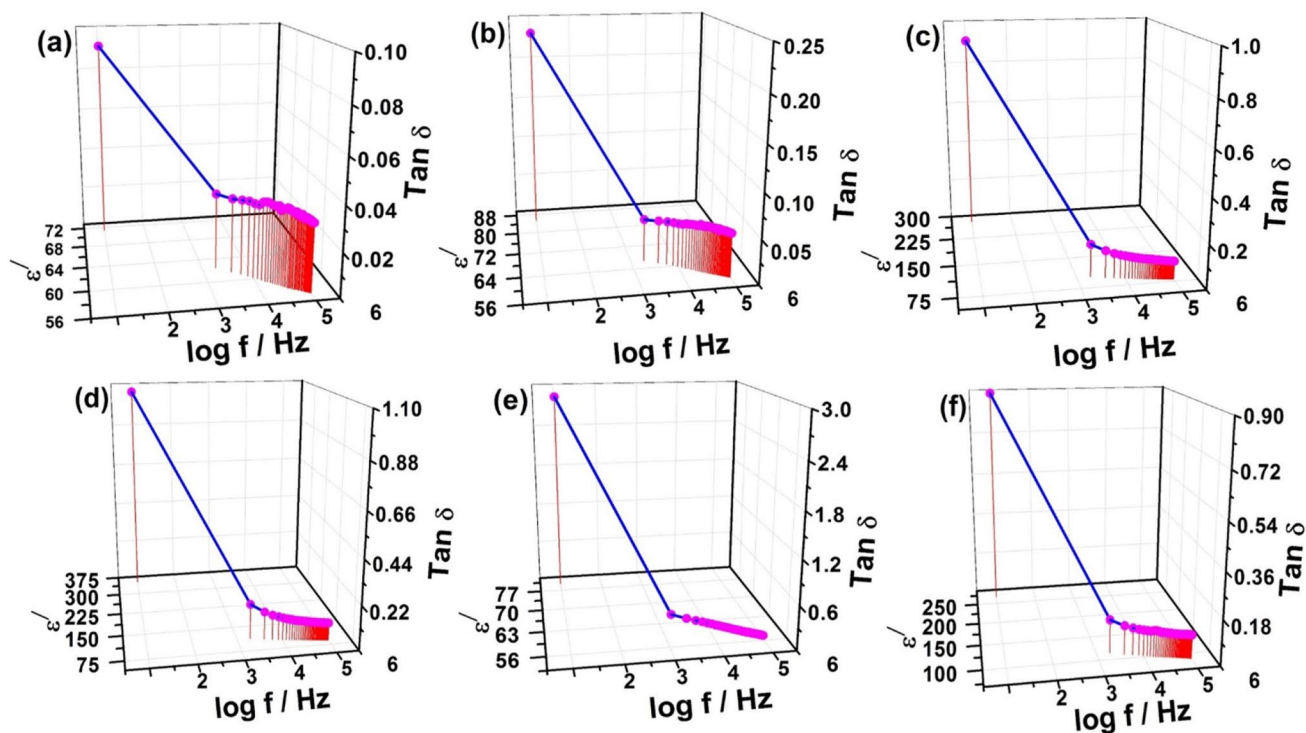


Fig. 9 Real part of dielectric permittivity and loss factor variation with frequency of transition metals incorporated ZnO–PVA polymer nanocomposites **a** ZnO–PVA, **b** ZnO–PVA–Cr₂O₃, **c** ZnO–PVA–Mn₂O₃, **d** ZnO–PVA–Fe₂O₃, **e** ZnO–PVA–NiO, and **f** ZnO–PVA–CuO

$$\epsilon'' = \epsilon' \tan \delta, \quad (9)$$

where ‘C’ presents the capacitance (F), ‘d’ is the thickness of the sample (m), ‘ ϵ_0 ’ is the permittivity of free space (8.85×10^{-12} F/m) and A is the area of the sample (m²). It can be seen that real and imaginary parts of dielectric permittivity decreased with the increase in frequency and turn out to be minimum at higher values of frequencies for all polymeric nanocomposite compositions. The highest values of dielectric permittivity at lower frequencies can be clarified by a well-known model of Maxwell–Wagner [30]. ZnO particles make semiconducting nanostructures in an insulating matrix of host PVA that assists in the formation of dipoles due to mismatch at interfaces. These dipoles become polarized in response to an externally applied field makes a significant contribution in inducing dielectric permittivity. The lower values of dipole relaxation time at higher frequencies attributed to the slight decrease in dielectric permittivity. On the other hand, relaxation time increases at higher frequencies and dipoles become no longer follow the external field. The value of real part of dielectric constant for ZnO/PVA was found as 74 which significantly enhanced up to 350 with the incorporation of transition metals oxide nanoparticles in matrix with the slight variation of loss factor. There are many reports on dielectric studies of ZnO/PVA and individual composites of transition metals incorporated

PVA matrix. The maximum reported approximate value of dielectric constant for relevant compositions yet found is 150 by El Sayed and El-Gamal [33] for Cr₂O₃ incorporated PVA composites. The comparison of findings of this work with previously reported values of dielectric permittivity and loss factor for similar type of compositions in literature is given in Table 4. The increase in dielectric permittivity with the incorporation of TM oxide nanoparticles might associate with the increment of charge carriers and interface areas. The quality of the dispersion of nanoparticles is another important factor affecting the dielectric permittivity of polymer nanocomposites. More agglomerations may provide a large hindrance in polarization in response to the external field and consequently induce lower dielectric permittivity with higher losses.

Figure 10b represents the variation of loss factor with frequency for all synthesized compositions. The loss factor shows the highest values at lower frequency regimes and decreases exponentially with the increase in frequency. The large values of loss factor at low frequencies follow the Maxwell–Wagner–Sillars polarization model [31], which associates it with the orientation of dipoles at interfaces for extremely low values of frequencies. The loss factor substantially decreases at higher frequencies due to a decrease in charge accumulation related to the fast periodic reversal of the external field which consequently lowers the oriented

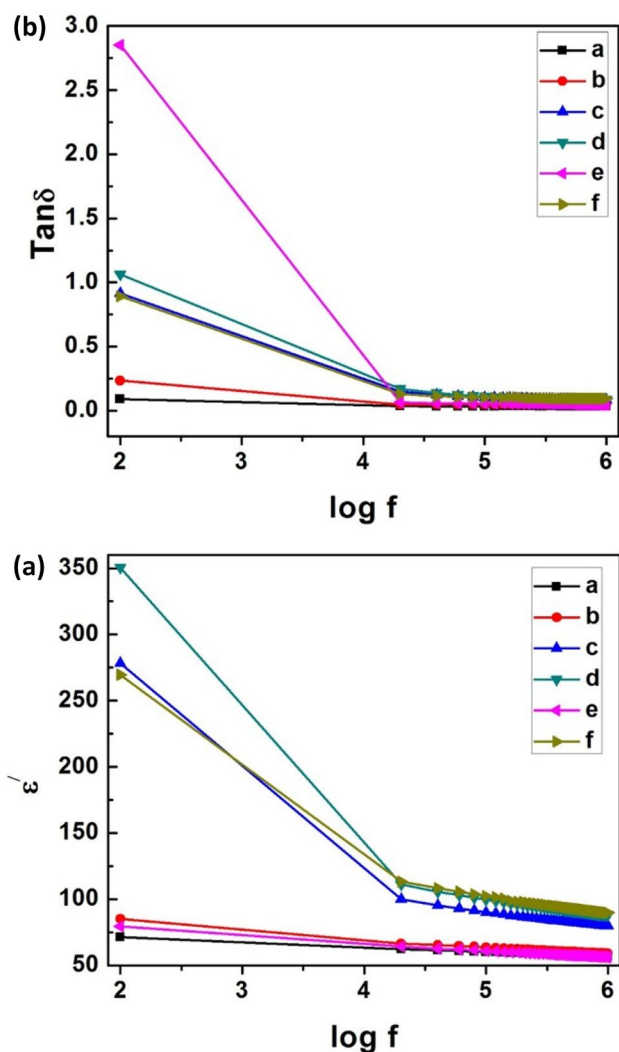


Fig. 10 Imaginary part of dielectric permittivity of transition metals incorporated ZnO–PVA polymer nanocomposites (a) ZnO–PVA, (b) ZnO–PVA–Cr₂O₃, (c) ZnO–PVA–Mn₂O₃, (d) ZnO–PVA–Fe₂O₃, (e) ZnO–PVA–NiO, and (f) ZnO–PVA–CuO

charge diffusion. AC conductivity of polymer nanocomposite samples was calculated using the following equation;

$$\sigma_{AC} = 2\pi f \epsilon'' \tag{8}$$

The variation of σ_{AC} was observed to increase with frequency followed the universal dielectric response law as presented in Fig. 11. The conductivity trend was found independent of the applied field at lower frequency regimes due to higher dispersion in the matrix while exponentially followed the field at higher frequencies. The lower values of band gap and higher AC conductivity of TM oxides

Table 4 Literature and reported values of dielectric parameters (ϵ' and $\tan\delta$) of different similar compositions and comparison with our findings

Authors	Materials studied	$\tan\delta$	ϵ'
Hassen et al. [16]	PVA–Cr ₂ O ₃	NA	58
Roy et al. [10]	PVA–ZnO	0.13	145
Hemalatha et al. [32]	PVA–ZnO	0.25	10
Rao et al. [18]	PVA–CuO	NA	8.5
El Sayed and El-Gamal [33]	PVA–Co ₃ O ₄	NA	150
Ambrosio et al. [8]	PVA–ZnO	1	80
Ningaraju et al. [17]	PVA–NiO	5	20
This work	PVA–ZnO	0.10	74
	PVA–ZnO–Cr ₂ O ₃	0.25	85
	PVA–ZnO–Mn ₂ O ₃	0.90	275
	PVA–ZnO–Fe ₂ O ₃	0.10	350
	PVA–ZnO–NiO	2.90	80
	PVA–ZnO–CuO	0.90	275

containing polymer matrix leads to the availability of more charge carriers for polarization hence provide enhanced dielectric permittivity with relatively low loss factors.

Conclusion

ZnO–PVA matrices were uniformly dispersed with synthesized TM oxide nanoparticles. Structural information reveals the presence of crystalline traces of corresponding nanoparticles with specific orientations in the polymer matrix. The energy band gap of ZnO–PVA was observed as 5.34 eV and found to decrease with the addition of TM oxide nanoparticles in the matrix. The least value of band gap 4.68 eV was estimated in iron oxide nanoparticles containing composition demonstrating the availability of more carriers for polarization in polymer nanocomposite. A sharp increase in dielectric permittivity was observed from 74 to 350 with comparatively low losses. The highest value of dielectric permittivity was observed in iron oxide nanoparticles incorporated ZnO–PVA polymer composite with a loss factor of 0.1. The lower values of band gap and higher AC conductivity of TM oxides containing polymer matrix lead to the availability of more charge carriers for polarization.

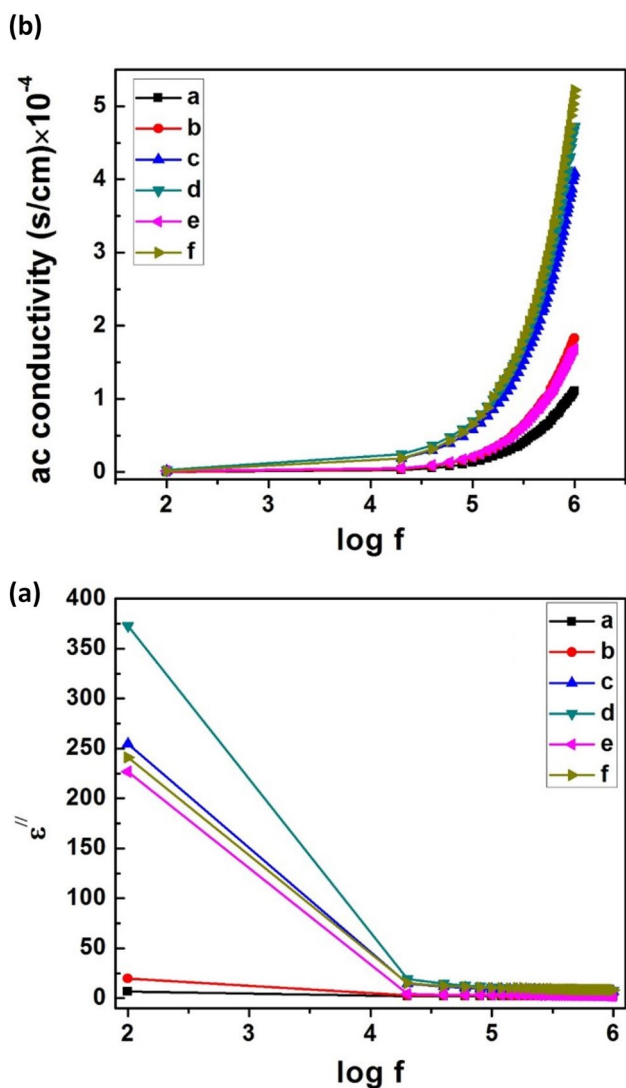


Fig. 11 Imaginary part and AC conductivity variation with frequency for transition metals incorporated ZnO–PVA polymer nanocomposites (a) ZnO–PVA, (b) ZnO–PVA–Cr₂O₃, (c) ZnO–PVA–Mn₂O₃, (d) ZnO–PVA–Fe₂O₃, (e) ZnO–PVA–NiO, and (f) ZnO–PVA–CuO

Acknowledgements The authors would like to extend his sincere appreciation to the Deanship of Scientific Research at King Saud University for funding the work through the Research Group Project No. RGP-VPP-311.

Compliance with Ethical Standards

Conflict of interest The authors declared that they have no conflict of interest.

References

- Mathen JJ, Madhavan J, Thomas A, Edakkara A, Sebastian J, Joseph J (2018) *J Mater Sci Mater Electron* 28:7190–7203
- Wang Z, Han NM, Wu Y, Liu X, Shen X, Zheng Q, Kim JK (2017) *Carbon* 123:385–394
- Xu X, Li Z, Wang J, Lin B, Ma W, Xia Y, Andersson MR, Janssen RAJ, Wang E (2018) *Nano Energy* 45:368–379
- Elkalashy O, Sheha E (2018) *Appl Phys A* 124:549
- Jayakumar A, Heera KV, Sumi TS, Joseph M, Mathew S, Praveen G, Nair IC, Radhakrishnan EK (2019) *Int J Biol Macromol* 136:395–403
- Viswanath V, Nair SS, Subodh G, Muneera CI (2019) *Mater Res Bull* 112:281–291
- Shanshool HM, Yahaya M, Yunus WM, Abdullah IY (2017) *Opt Quantum Electron* 49:18
- Ambrosio R, Carrillo A, Mota MDLL, Torre KDL, Torrealba R, Moreno M, Vazquez H, Flores J, Vivaldo I (2018) *Polymers* 10:1370
- Ebnalwaled AA, Ismaiel AM (2019) *Measurement* 134:89–100
- Roy AS, Gupta S, Sindhu S, Ramamurthy CP (2013) *Composites* 47:314–319
- Sekar AD, Muthukumar H, Chandrasekaran NI, Matheswaran M (2018) *Chemosphere* 205:610–617
- Bakhtiari SSE, Karbasi S, Tabrizi SAH, Kahrizsangi RE (2019) *Polym Compos* 40:E1622–E1632
- Abutalib MM (2019) *Physica B* 557:108–116
- Choudhary S, Sengwa RJ (2018) *Curr Appl Phys* 18:1041–1058
- Hashmi HS, Raizada A, Madhu GM, Kittur AA, Suresh R, Sudhina HK (2015) *Plast Rubber Compos* 44:33–39
- Hassen A, El Sayed AM, Morsi WM, El-Sayed S (2012) *J Appl Phys* 112:093525
- Ningaraju S, Prakash APG, Ravikumar HB (2018) *Solid State Ion* 320:132–147
- Rao JK, Raizada A, Ganguly D, Mankad MM, Satayanarayana SV, Madhu GM (2015) *J Mater Sci* 50:7064–7074
- Abbas K, Aslam MA, Amir M, Atiq S, Ahmed Z, Siddiqi SA, Naseem S (2017) *J Alloys Compd* 712:720–731
- Aslam M, Kalyar MA, Raza ZA (2019) *Polym Bull* 76:73–86
- Hemalatha KS, Rukmani K, Suriyamurthy N, Nagabhushan BM (2014) *Mater Res Bull* 51:438–446
- Fernandes DM, Hechenleitner AAW, Lima SM, Andrade LHC, Caires ARL, Pineda EAG (2011) *Mater Chem Phys* 128:371–376
- Heiba ZK, Mohamed MB (2019) *J Mol Struct* 1181:507–517
- Shah J, Ranjan M, Sooraj KP, Sonvane Y, Gupta SK (2019) *J Mol Liq* 283:550–557
- Shanshool HM, Yahaya M, Yunus WMM, Abdullah IY (2016) *J Mater Sci Mater Electron* 27:9804–9811
- Mohammed MJ, Rasheed ZS, Hassan AS (2018) *Nanocomposites* 23:118–123
- Selvi J, Mahalakshmi S, Parthasarathy V, Hu C, Lin YF, Tung KL, Anbarasan R (2019) *Polym Compos* 40:3737–3748
- Maji P, Choudhary RB, Majhi M (2018) *Appl Phys A* 124:70
- Kumar GV, Chandraman R (2009) *Appl Surf Sci* 255:7047–7705
- Bouropoulos N, Psarras GC, Moustakas N, Chrissanthopoulos A, Baskoutas S (2008) *Phys Status Solidi A* 205:2033–2037
- Latif I, Al-Abodi EE, Badri DH, Khafagi JA (2012) *J Am Polym Sci* 2:135–140
- Hemalatha KS, Sriprakash G, Prasad MVNA, Damle R, Rukmani K (2015) *J Appl Phys* 118:154103
- El Sayed AM, El-Gamal S (2015) *J Polym Res* 22:97

Publisher's Note Springer Nature remains neutral with regard to jurisdictional claims in published maps and institutional affiliations.